Research Article Vol. 30, No. 3 / 31 Jan 2022 / Optics Express 3729

Optics EXPRESS

Detecting multiple chiral centers in chiral molecules with high harmonic generation

OFER NEUFELD,[1,2,4] OMRI WENGROWICZ,[2] OR PELEG,[2] ANGEL RUBIO,[1,3] AND OREN COHEN[2,5]

[1] *Max Planck Institute for the Structure and Dynamics of Matter and Center for Free-Electron Laser Science, Hamburg 22761, Germany*
[2] *Technion – Israel Institute of Technology, Physics Department and Solid State Institute, Haifa 3200003, Israel*
[3] *Center for Computational Quantum Physics (CCQ), The Flatiron Institute, New York, NY 10010, USA*
[4] *oneufeld@schmidtsciencefellows.org*
[5] *oren@technion.ac.il*

Abstract: Characterizing chiral is highly important for applications in the pharmaceutical industry, as well as in the study of dynamical chemical and biological systems. However, this task has remained challenging, especially due to the ongoing increasing complexity and size of the molecular structure of drugs and active compounds. In particular, large molecules with many active chiral centers are today ubiquitous, but remain difficult to structurally analyze due to their high number of stereoisomers. Here we theoretically explore the sensitivity of high harmonic generation (HHG) to the chiral of molecules with a varying number of active chiral centers. We find that HHG driven by bi-chromatic non-collinear lasers is a sensitive probe for the stereo-configuration of a chiral molecule. We first show through calculations (from benchmark chiral molecules with up to three chiral centers) that the HHG spectrum is imprinted with information about the handedness of each chiral center in the driven molecule. Next, we show that using both classical- and deep-learning-based reconstruction algorithms, the composition of an unknown mixture of stereoisomers can be reconstructed with high fidelity by a single-shot HHG measurement. Our work illustrates how the combination of non-linear optics and machine learning might open routes for ultra-sensitive sensing in chiral systems.

© 2022 Optica Publishing Group under the terms of the Optica Open Access Publishing Agreement

1. Introduction

Chirality is a ubiquitous property in nature. It manifests in a plethora of physical and chemical systems ranging from fundamental particles [1], to galaxies [2], and materials [3–5]. In biology and medicine, chirality plays an essential role in determining the body's physiological response to drug administration. This is a direct consequence of the inherent chirality of biologically active molecules such as DNA and amino acids [6,7]. A major task in modern drug development is thus to identify, classify, and separate, the different chiral constituents of molecules to a high precision [8,9]. In fact, a new drug cannot receive FDA approval until a sufficiently pure mixture has been synthesized and characterized [10]. However, this task has become exponentially difficult ever since drug development has moved towards larger biological molecules and chemical species that possess a high number of active chiral centers (stereocenters, see illustration in Fig. 1). 'Multi-center' molecules have a total of 2N stereoisomers (isomers of the same chiral molecule that differ only by the handedness around each chiral center) to be separated, where N is the number of stereocenters [9]. Notably, characterization of chirality in multi-center molecules is a very challenging task, because no single standard all-optical measurement is sufficient. For instance, circular dichroism (CD) spectroscopy [11] (which is the workhorse of the pharmaceutical industry) cannot characterize a mixture of four or more stereoisomers (i.e $N > 1$), because signals from different stereoisomers can either cancel out or be indistinguishable.

#445743 https://doi.org/10.1364/OE.445743
Journal © 2022 Received 12 Oct 2021; revised 7 Jan 2022; accepted 7 Jan 2022; published 20 Jan 2022

Optics EXPRESS

Instead, current approaches rely on an ad-hoc combination of multiple measurements from both optical and chemical methods, which are not always transferable and can be very time-consuming.

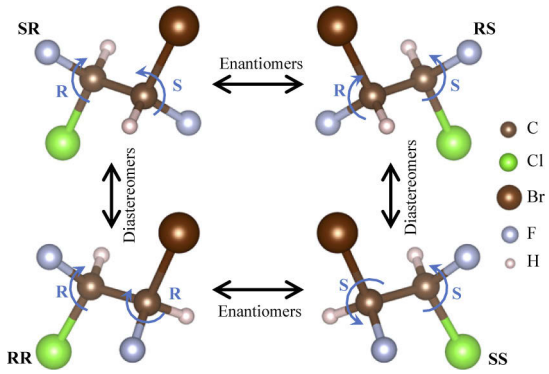

Fig. 1. Schematic illustration of the two-center chiral system showing all four stereoisomers of chiral molecules for $C_2H_2BrClF_2$. The arrows indicate enantiomeric pairs of molecules that are mirror images of one another, as well as diastereomers that are not connected by a mirror symmetry. Labeling of the chiral center is around the two carbons in the chain, respectively, e.g. 'RS' labels a chiral molecule with 'R' configuration around the 1st carbon, and 'S' around the 2nd.

In this context, recent years have seen an explosion of all-optical chirality characterization methods of enhanced sensitivity, including second-order nonlinear optical methods [11–16], enantio-specific state transfer [17], and methods based on high harmonic generation (HHG) [18–25]. However, these studies considered only a single chiral center (except a single study that considered two chiral centers but only in aligned chiral media [26]), and it is not clear how, or if, these methods can be extended to probe the structure of multi-center molecules.

Here we theoretically demonstrate all-optical chiral spectroscopy for multi-center molecules utilizing strong lasers and HHG. We employ bi-chromatic laser fields that are non-collinearly aligned and possess an optical property called 'local-chirality' [21] (which has been recently shown to be effective for probing single-center chiral molecules [21,22,27]). We find that this configuration leads to large chiral signals between different stereoisomers of molecules with multiple chiral centers. In particular, the extreme non-linear nature of the HHG process imprints, with a high selectivity, unique fingerprints of the handedness and structure of each chiral center onto the harmonic spectra, allowing the stereoisomers to be distinguished by harmonic power measurements. By simultaneously measuring several harmonic orders, this scheme can be applied to characterize the composition of an unknown mixture of stereoisomers with high precision, where the reconstruction is performed in a single-shot measurement that is fed into an algorithm that we developed (either classical or deep learning based).

2. Methodology

2.1. High harmonic generation calculations

We begin by describing the methodology used in numerical calculations. Calculations were performed with two sets of benchmark chiral molecules with two and three chiral centers localized on carbon atoms. The two-center chiral molecular system was chosen to be 1-Bromo-2-chloro-1,2-difluoroethane ($C_2H_2BrClF_2$, see Fig. 1), while the three-center chiral molecular system was chosen as 2-Bromo-4-chloro-3-fluoropentane (C_5H_9BrClF, see Supplement 1 (SM) for illustration). These molecules are linear alkanes with substituted hydrogens, where each carbon atom with four non-identical substituents forms an active stereocenter. Each molecule is labeled

Optics EXPRESS

according to the handedness of its stereocenters, e.g. 'RS' refers to the two-center chiral molecule with handedness 'R' about the first center and 'S' about the second (see illustration in Fig. 1).

The ground states of the molecules were obtained from density functional theory (DFT) with the real-space grid-based OCTOPUS code [28–30] within the local density approximation (LDA) for the exchange-correlation (XC) functional with an added self-interaction correction (SIC) [31]. Technical details of these calculations are specified in the SM.

For each isomer, HHG calculations were subsequently performed within the single active electron (SAE) approximation for the highest occupied molecular orbital (HOMO) in the length gauge, governed by a time-dependent Schrödinger equation (TDSE) given in atomic units by:

$$i\frac{\partial}{\partial t}|\psi_\Omega(t)\rangle = \left[-\frac{1}{2}\nabla^2 + V_\Omega(\mathbf{r}) + \mathbf{E}(t)\cdot\mathbf{r}\right]|\psi_\Omega(t)\rangle \tag{1}$$

where $|\psi_\Omega(t)\rangle$ is the SAE wave function that at $t=0$ was taken as the Kohn-Sham (KS) HOMO orbital, $\mathbf{r}$ is the electron's coordinate, and $V_\Omega(\mathbf{r})$ is the effective potential felt by the SAE that includes both the ionic potential and screening effects from deeper orbitals at a fixed molecular orientation, Ω. $V_\Omega(\mathbf{r})$ was taken as the KS potential of the ground state system:

$$V_\Omega(\mathbf{r}) = -\sum_I \frac{Z_I}{|\mathbf{R}_I - \mathbf{r}|} + \int d^3r' \frac{\rho_\Omega(\mathbf{r})}{|\mathbf{r}-\mathbf{r}'|} + v_{XC}[\rho_\Omega(\mathbf{r})] \tag{2}$$

where Z_I is the charge of the I'th nuclei and $\mathbf{R}_I$ is its coordinate, v_{XC} is the XC potential that is a functional of $\rho_\Omega(\mathbf{r})$, the ground state electron density for that particular orientation. Effectively, the above numerical procedure is equivalent to performing time-dependent DFT calculations, but where the KS potential is frozen to its ground state form, leading to the independent particle approximation, and where only the HOMO KS state is propagated in time. The SAE method is standardly applied in HHG since it is capable of making qualitative predictions while maintaining numerical feasibility, which is why it is employed in our study of larger multi-center chiral molecules. It is also further motivated by the low ionization probability in our explored systems, and since deeper orbital contribute exponentially less to the HHG yield (there are no degenerate orbitals in the chiral molecules). $\mathbf{E}(t)$ in Eq. (1) denotes the time-dependent laser electric field of the ω-2ω bi-chromatic non-collinear laser configuration:

$$\mathbf{E}(t) = E_0 A(t)\mathrm{Re}\{e^{i\omega t + i\eta}\hat{\mathbf{e}}_1 + \Delta e^{2i\omega t}\hat{\mathbf{e}}_2\} \tag{3}$$

where E_0 is the electric field amplitude of the ω beam, Δ is the amplitude ratio between the beams, η is a relative phase, $\hat{\mathbf{e}}_{1,2}$ are unit vectors along the polarization direction of each beam (each beam is circularly-polarized and counter-rotating, but propagating with a small opening angle α w.r.t the z-axis), $A(t)$ is a dimensionless envelope function (taken to be trapezoidal with two-cycle rise and drop sections and a four-cycle flat-top). Note that we have applied the dipole approximation and neglected all spatial degrees of freedom in $\mathbf{E}(t)$. Calculations were thus performed microscopically at the focus of both beams where they overlap spatially and temporally. While this approximation is not strictly valid for non-collinear beams (since the phase of $\mathbf{E}(t)$ can change across the interaction region and lead to phase matching issues), such issues can be avoided either by employing a thin interaction region (which is possible both in gas or liquid phases [32,33]), or by controlling the relative phases between the beams [21,22].

Equation (3) describes two noncollinear circularly polarized laser beams of frequencies ω and 2ω, which are focused together into a randomly-oriented chiral media (as illustrated in Fig. 2). For α=0 one recovers the collinear planar form of $\mathbf{E}(t)$ (i.e. the field is polarized in the *xy* plane) and $\mathbf{E}(t)$ reduces to a counter-rotating bi-circular field [34–36], as has been utilized to generate circularly-polarized high harmonics [37,38]. For α≠0 one obtains a locally-chiral field with a nonzero degree of chirality (DOC) [39]. This field has a unique property of being distinct from

Optics EXPRESS

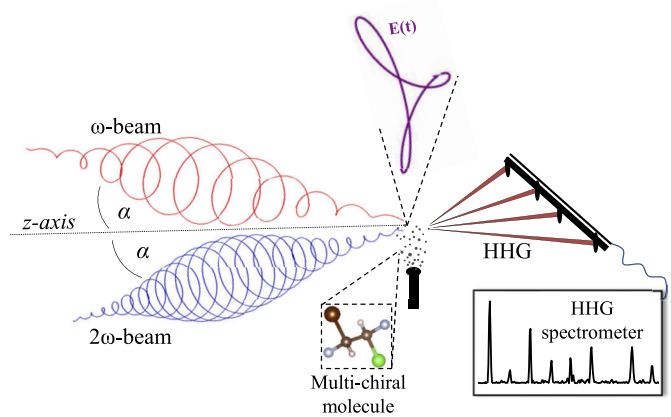

Fig. 2. Schematic illustration of the ω-2ω (bi-chromatic) driving field and suggested experimental set-up for chiral mixture reconstruction. The field is comprised of two strong laser beams that are focused together into a mixture of randomly oriented chiral molecules with several stereoisomers (the mixture can either be in liquid or gas phase). The beams have an opening angle (2α) relative to their propagation axes and are circularly polarized in order for the total electric field to exhibit a non-zero degree of chirality [21,39]. High harmonics from the medium are emitted in different angles in space and their powers and polarizations are measured, and then inputted into an algorithm that reconstructs the composition of the mixture.

its mirror image within the dipole approximation, which leads to strong chiral signals in the nonlinear optical response [21].

The TDSE in Eq. (1) was solved within OCTOPUS code (further technical details are found in the SM) for each molecular orientation w.r.t the driving laser field. From the obtained $|\psi_\Omega(t)\rangle$ we calculated the time-dependent dipole acceleration:

$$\mathbf{a}_\Omega(t) = \frac{\partial^2}{\partial t^2}\langle\psi_\Omega(t)|\mathbf{r}|\psi_\Omega(t)\rangle \tag{4}$$

We performed orientation averaging for each isomer to describe randomly oriented chiral media, where the angle Ω was integrated over with trapezoidal weights on an Euler grid in a method similar to that used in Ref. [27] with a total of 208 non-equivalent angular orientations (405 total orientations). From this integration, we obtained the dipole acceleration of each randomly oriented molecular isomer:

$$\mathbf{a}(t) = \int d\Omega\, \mathbf{a}_\Omega(t) \tag{5}$$

The HHG spectra were obtained as a Fourier transform of $\mathbf{a}(t)$. For a mixture of different stereoisomers, the HHG spectra was calculated as a coherent sum of the spectra from all isomers in the solution with appropriate weights (according to their individual concentrations).

2.2. Chirality reconstruction algorithms

In order to reconstruct the compositions of unknown mixtures of isomers, we developed two algorithmic approaches. The first is based on a classical steepest descent approach, while the second relies on deep learning. Within both approaches, the measured HHG yields for several harmonic orders from a mixture of stereoisomers are inputted into the algorithm. The algorithms output the reconstructed weights for the concentrations of each isomer in the mixture, where

Optics EXPRESS

it is assumed that the mixture only contains stereoisomers of that particular species (though this constraint could be relaxed in future works). We have simulated many random realizations of mixtures, and quantified the success of the method by comparing the reconstructed weights with the ground truth. The robustness of the method was tested by reconstructing mixture compositions while including random noise in the input data.

We now specify the details of both approaches. The classical approach was implemented in MATLAB [40]. It searches for the optimal molar concentrations of each constituent in the mixture by minimizing a target function defined as the difference between the measured yields, and the reconstructed yields. For each harmonic order we define the target function:

$$f_{tar}{}^{(h)}(\mathbf{c}) = I_{mix}{}^{(h)} - \left| \sum_{j=1}^{M} c_j \sqrt{I_j{}^{(h)}} e^{i\phi_{1j}^{(h)}} \right|^2 \tag{6}$$

where the molar concentrations are labeled as c_j (forming the vector $\mathbf{c}$), "j" is the index of the stereoisomer running from 1 to 2^{N} (N is the number of chiral centers in the molecule and we denote $\mathrm{M} = 2^{\mathrm{N}}$). $I_{mix}{}^{(h)}$ is the input integrated yield of the h'th harmonic from the unknown mixture, which is taken from the HHG simulations. $I_j{}^{(h)}$ is the integrated intensity of the h'th harmonic from the j'th isomer, and $\phi_{1j}^{(h)}$ is the relative phase of the h'th harmonic between the 1'st and the j'th isomer (where $\phi_{11}^{(h)}$=0). For the classical steepest descent approach, both of these quantities are assumed to be known reference data that the algorithm has access to. In an experimental set-up, this reference data can be obtained directly from HHG measurements from the pure isomer compounds, as well as 50/50 mixtures of all isomer pairs (while here they are taken directly from the HHG calculations). An overall target function is defined by summing the errors from all harmonics in a subset K:

$$F_{tar}(\boldsymbol{c}) = \sum_{h \epsilon K} |f_{tar}{}^{(h)}(\boldsymbol{c})| \tag{7}$$

The molar concentrations formally uphold the following constraints that are applied in the algorithm: $1 = \sum_{i=1}^{M} c_i$, which is used to determine: $c_M = 1 - \sum_{i=1}^{M-1} c_i$ (reducing the number of parameters to reconstruct from M to M-1). Also, each c_i upholds: $0 \leq c_i \leq 1$. This approach essentially searches for a global minimum for $F_{tar}(\boldsymbol{c})$ with respect to M-1 parameters; thus, reasonable solutions are expected when utilizing at least M-1 harmonic orders for the reconstruction process.

The deep learning approach is implemented in Pytorch [41] and is comprised of two modules. The first module is denoted as HHGNet, which models the measurement process. It is a non-parametric module (non-trained) that is used to generate the expected yields from a given simulated mixture of isomers. The simulated spectrum is converted to logarithmic scale and normalized in the range [-1,1], and is then fed as input into the second module, denoted as MuChiNet. This module is trained to estimate the molar concentrations corresponding to the input yields. It is comprised of two 1D convolution layers, each followed by a MaxPool and a ReLU nonlinearity, and four fully connected layers, each followed by a ReLU nonlinearity [42]. The output is normalized by a softmax layer such that the sum of concentrations gives the physical 100%, which is comparable to the ground truth. The Adam optimizer [43] is used to train the network over 1000 random simulated samples (which are fully-independent from the subsequently used testing set). Crucially, within this technique the relative phases for each harmonic order between isomers ($\phi_{1j}^{(h)}$) are not used as input, significantly simplifying the experiment

Optics EXPRESS

3. Results and discussion

3.1. Stereocenter sensitivity in HHG

With the approach described above, we investigate HHG from multi-chiral molecules, starting with the model two-center chiral system. Figures 3(a,b) present exemplary HHG spectra from the various stereoisomers of $C_2H_2BrClF_2$ driven by locally-chiral light (with α=7.5°), where enantiomer pairs are plotted together. The HHG spectra show large enantio-discrimination between pairs of enantiomers, especially for higher harmonics. The size of the discrimination can be quantified by defining a chiral dichroism (CD, not to be confused with circular dichroism) per harmonic order h as:

$$CD^{(h)} = 2\frac{I_j^{(h)} - I_k^{(h)}}{I_j^{(h)} + I_k^{(h)}} \tag{8}$$

where j,k indicate indices for the various stereoisomers (e.g. in this case j = RR,SS,RS,SR) and $I_j^{(h)}$ is the integrated harmonic yield for the h'th harmonic order from the j'th isomer. The CD in Eq. (8) is normalized from -200 to 200% and is a measure for the sensitivity of HHG to the stereo-configuration. For the particular parameters in Fig. 3 we obtain CDs of ∼20% for enantiomeric pairs. In the semi-classical picture for HHG, the strong CDs can generally be thought of as arising from the separate contributions of the ionization, propagation, and recombination, sub-processes. However, the role of each of these in the overall CD is somewhat obscured in the orientation averaged medium. Nonetheless, we can rule out any strong CD originating from the ionization sub-process, because CDs in the ionization rates from mirror enantiomers are too small in our examined conditions to account for the large values obtained in HHG. We hypothesize that a combination of the propagation and recombination steps underlie the strong chiral response in our case (since these sub-processes probe the long-range chiral potential, and chiral orbitals, respectively).

Figures 3(c,d) present similar HHG spectra, but showing only the y-polarized emitted power. This simulates a set-up where harmonics are passed through a polarizer before entering the spectrometer, which can enhance the CD substantially – for the particular example in Fig. 3 the CD increases on average by a factor of about two after the polarizer. Thus, from this point on we only refer to CD that is obtained with a y-polarizer, and only the y-polarized HHG spectra is used for reconstructions.

Notably, discrimination between stereoisomers that are not enantiomers but are diastereomers (i.e. are not exact mirror images of one another, see illustration in Fig. 1) is even more efficient. The different structures of diastereomers imprint robust unique features onto the HHG spectra, including the plateau structure and cutoff position. CDs for diastereomers in Fig. 3 for instance are on order of ∼100%.

We further analyze the CD between different stereoisomers with respect to the laser conditions. A main degree of freedom here is the opening angle between the beams, α. Figure 4 shows the CD values vs. α for the different harmonic orders between the different isomers. For enantiomer pairs, the CD increases almost linearly with α starting from α=0 (see Fig. 4(a,b)). This behavior is in correspondence with the properties of the driving bi-chromatic laser that vary with α: (i) for α=0 we have a co-planer bi-circular driving field where every third harmonic is suppressed due to symmetry [44,45]. In this geometry the field is not locally-chiral due to its planar nature, which leads to zero CD. (ii) As α increases the DOC in the driving field increases linearly [39]. Thus, Fig. 4(a,b) indicates that there is a correspondence of HHG chiral signals with light's DOC, which has also been recently reported for photoelectrons [27]. This is maybe surprising due to the highly nonlinear nature of the process. We hypothesize that the origin of the effect lies in the orientation averaging from the full molecular ensemble, which might reduce this strong nonlinear connection to a linear one (at least in the perturbative small DOC regime). We expect

Optics EXPRESS

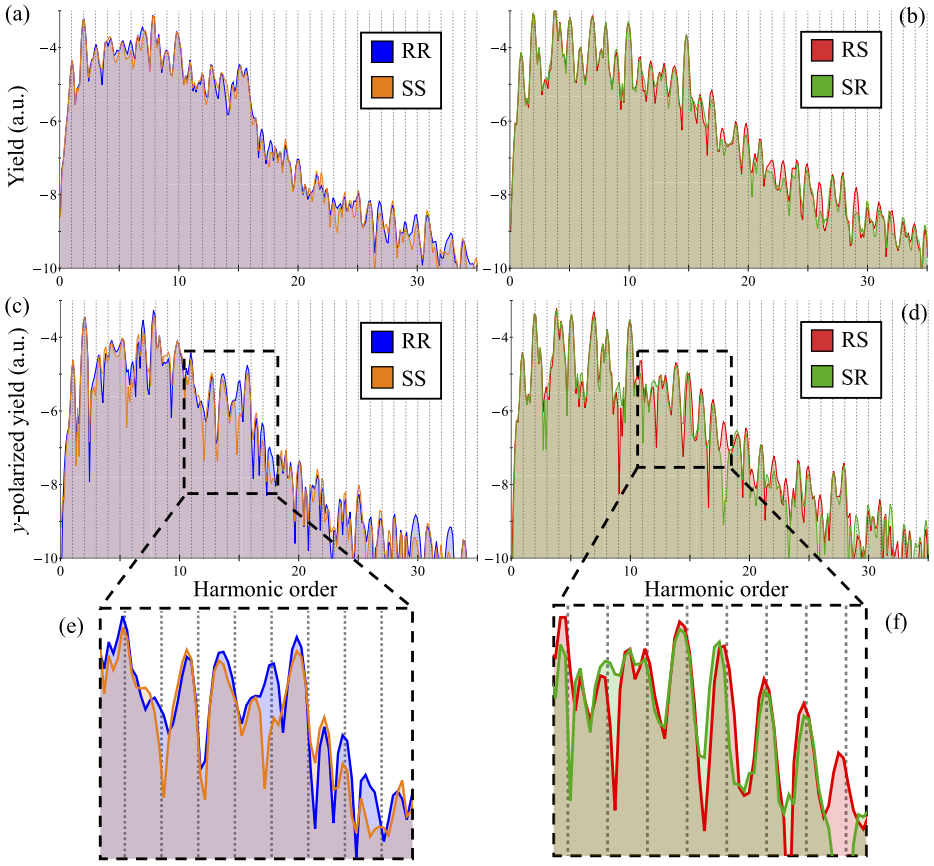

Fig. 3. Extreme nonlinear response and harmonic emission from two-center chiral system, $C_2H_2BrClF_2$. (a,b) HHG power spectra from pairs of enantiomers, showing that the harmonic power is selective to the stereo-configuration of the system. Dashed lines represent integer harmonic orders. (c,d) Same as (a,b) but for y-polarized spectral power which shows stronger stereo-selectivity. (e,f) Zoom-ins on regions of interest in the HHG spectra with high CD from (c,d), respectively. Plot calculated for the laser parameters: λ=1400nm, $I_0 = 10^{13}$ W/cm^2, α=7.5°, η=0, Δ=1/$\sqrt{2}$.

that this linear connection should break down eventually due to an interplay of the increase in the DOC with α, and the decrease in the recombination cross-section with α, which should lead to a saturation effect as is already visible for some harmonics in Fig. 4(a,b). It is also interesting to discuss the dependence of the CD on the particular harmonic order. A general trend visible in Fig. 4(a,b) is that harmonics in the plateau region (and also cutoff region) tend to reach higher CD values, especially compared to the perturbative region. This indicates the importance of the propagation sub-process in HHG for obtaining high CDs from locally-chiral light.

Another point to note is that the CD between diastereomers is mostly independent of the beams opening angle (see Fig. 4(c,d)). This suggests that the ability to separate diastereomers in HHG is largely independent of light's chirality, and is instead a consequence of the extremely nonlinear nature of the interaction that is sensitive to the chemical properties of the system (e.g. orbital and potential energy structure). We also note that few harmonics in Fig. 4(c,d) do show strong dependence on α, which is a consequence of interference effects (the electron trajectories are altered with α, changing their relative phases).

Optics EXPRESS

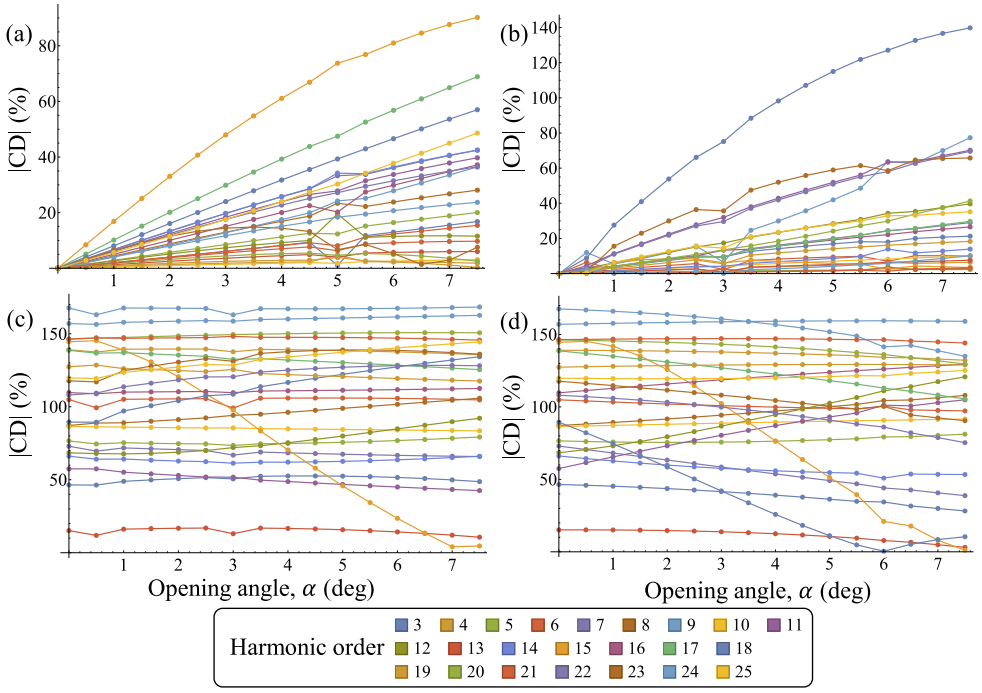

Fig. 4. Chiral dichroism from two-center multi-chiral system vs. the bi-chromatic field opening angle, α. (a) CD per harmonic order between the enantiomers RR and SS of $C_2H_2BrClF_2$. (b) Same as (a) but for the enantiomers RS and SR. (c) same as (a,b) but for the diastereomers RR and RS. (d) Same as (c) but for the diastereomers RR and SR. Plot calculated for the same laser parameters as Fig. 3, but where α is varied up to 7.50.

Next, we perform calculations in the benchmark three-center chiral molecular system, C_5H_9BrClF. Figure 5 shows exemplary HHG spectra from the various stereoisomers of C_5H_9BrClF, which clearly indicates the strong selectivity persists even in molecules with a high number of chiral centers. Figure 5(e,f) shows that CD values range around 30% for enantiomeric pairs, and 80% for diastereomers, similarly to the two-center system. The fact that each stereoisomer leads to unique fingerprints in the harmonic spectra, as well as very large CDs, opens the possibility for characterization schemes based on HHG, as we will show in the next section.

3.2. Reconstruction of chiral mixtures

We have simulated the response of random sets of mixtures of stereoisomers, and employed our developed reconstruction algorithms (classical- and deep-learning-based) to retrieve the molar concentrations of the mixtures. Results for both the two- and three-center multi-chiral molecules are presented in Fig. 6 from both algorithms, where the reconstruction utilizes the y-polarized harmonic power that was shown to produce better selectivity (utilizing 20 harmonics in each case). The reconstruction error in a given simulated mixture is calculated as the mean error between the ground truth and the reconstructed concentrations of all stereoisomers. Statistics of errors is obtained for 500 simulated mixtures, from which the mean error and the standard deviation of the error are calculated. Noise was introduced as random errors in the harmonic powers of the calculated HHG spectra from the simulated mixture (i.e. that inputted into the reconstruction algorithm).

Figure 6(a,b) shows mixture concentration reconstruction data from the classical algorithm, which is robust to random noise in the harmonic power data – reconstructions as good as 1%

Optics EXPRESS

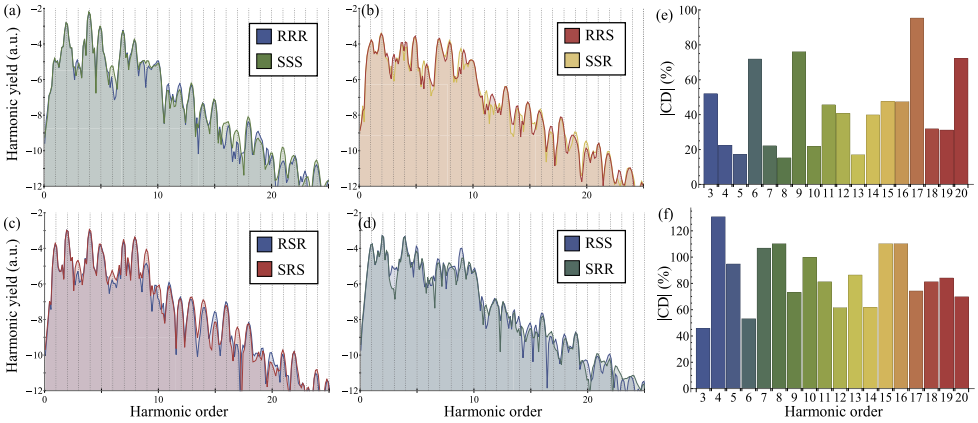

Fig. 5. HHG and chiral dichroism from the three-center multi-chiral system, C_5H_9BrClF. (a-d) *y*-polarized HHG power spectra for the various stereoisomers of C_5H_9BrClF, where enantiomer pairs are plotted together. (e) |CD| per harmonic order between enantiomer pairs (averaged over all pairs – RRR/SSS, RRS/SSR, RSS/SRR, RSR/SRS). (f) Same as (e) but averaged over all diastereomer pairs. Plots calculated for the same laser parameters as Fig. 3, but for λ=800nm.

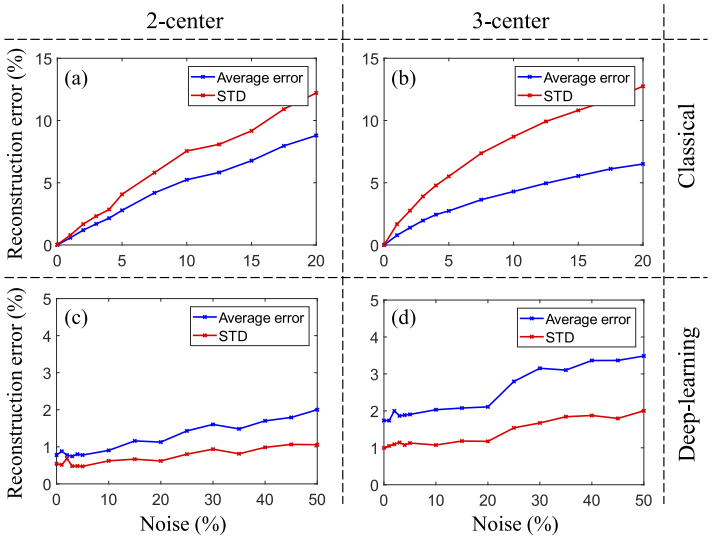

Fig. 6. Algorithmic reconstruction of stereoisomer concentrations in unknown mixtures of chiral molecules. (a) Reconstruction statistics vs. noise in harmonic power for two-center multi-chiral molecule using the classical algorithm. Statistics is obtained by simulating 500 random mixtures for every noise level. The absolute error is calculated by averaging the error over all realizations and over all isomers for a given mixture. (b) Same as (a) but for the three-center chiral system. (c,d) Same as (a,b) but with the deep-learning algorithm. Note that the axes scales are different in the classical and deep-learning approaches.

are obtained for noise levels up to 1% for both the two- and three-center multi-chiral molecules. Importantly, the reconstruction quality and noise robustness almost does not change between the two-center and three-center system, indicating that the method should be highly applicable to even larger complex molecular structures.

Optics EXPRESS

For optimization purposes, one may also consider optimizing the chosen subset of measured harmonic orders that are fed into the algorithm (the subgroup K in Eq. (7)). For instance, one might expect that harmonics that show stronger dichroism between pure enantiomer pairs would increase the signal to noise ratio and reduce reconstruction uncertainties. We have tested various such schemes, but generally observed weak dependence of the reconstruction quality with respect to the harmonic input data, as long as roughly the same number of harmonics were utilized for the reconstruction. On the other hand, by measuring more harmonic orders the reconstruction error can indeed be reduced, as expected (not presented).

We highlight that the stereocenter specificity in Fig. 6 is not possible with standard all-optical methods such as circular dichroism absorption spectroscopy, further emphasizing the importance of the suggested method. One particular example that stresses this difference is a mixture of chiral molecules with equal concentrations for each of the enantiomeric pairs of the stereoisomers, for instance, a mixture comprised of equal parts of all constituents (e.g. 25% for each RR, SS, RS, SR in the two-center system). In this case, the total mixture is racemic, making it completely inaccessible with standard chiroptical techniques regardless of the number of measurements performed. In contrast, our approach successfully reconstructs the concentration of each constituent to a high precision, and works just as well as it does in any other mixture.

Figures 6(c,d) present similar reconstruction data using the deep-learning algorithm. Reconstructions are generally at the same level of quality, or better, than those obtained with the classical approach for low noise levels. At first glance this may seem like a disappointing result, because one expects the deep learning approach should greatly out-perform the classical algorithms for global minimization. However, we recall that the classical approach in Fig. 6(a,b) assumed that the harmonic phases are known reference data that the algorithm has access to, while the deep-learning approach does not utilize this data. In that respect, the deep-learning scheme has the potential for enhanced realizations in an experimental set-up, provided that one can obtain high quality training data. We also note that the deep-learning approach is more robust over much more noisy data sets, with errors below 4% even up to 50% noise. On the other hand, it tends to lead to an average of 1% errors even in the absence of noise, which is attributed to the lack of phase information (whereas in the classical approach at zero noise the reconstruction equations are exactly solvable, leading to vanishing errors in reconstruction). We emphasize that these results can likely be optimized by improving the algorithmic schemes.

4. Conclusions

To summarize, we have theoretically shown that HHG with 'locally-chiral' light (with bi-chromatic non-collinear lasers [21,39]) is a sensitive probe for molecular chirality and handedness in chiral molecules with multiple stereocenters. The extreme nonlinear nature of the process allows distinguishing between enantiomers and diastereomers, where unique fingerprints of each isomer are imprinted onto the harmonic power and its polarization state. This result allows utilizing HHG for obtaining all-optical characterization of mixtures of chiral molecules (either in gas or liquid phases) to a high precision, in a single-shot measurement. We have simulated the reconstruction process with both classical- and deep-learning-based algorithms, showing that high quality and robust reconstructions can be obtained.

Our results numerically demonstrate the first all-optical method for analyzing chiral molecules with multiple active chiral centers. Notably, while we explored here simpler benchmark alkane multi-chiral systems, the mechanism responsible for the chiral signal generation and detection should also be valid in larger bio-molecular complexes, and even including other effects of multiple active orbitals and active vibrational modes. Thus, we are hopeful that the technique would be transferable to such interesting systems (even if requiring more complex reconstruction algorithms). Looking forward, our work could be used for deriving novel chirality spectroscopy

Optics EXPRESS

techniques in topological [46,47] and dynamical [48,49] systems based on the combination of extreme nonlinear optics and artificial intelligence.

Funding. Schmidt Family Foundation; Rhodes Scholarships; Alexander von Humboldt-Stiftung; Israel Academy of Sciences and Humanities; European Research Council (819440-TIMP, ERC-2015-AdG-694097).

Acknowledgments. We acknowledge financial support from the European Research Council (ERC) grant ERC-2015-AdG-694097, and the ERC under the European Union's Horizon 2020 research and innovation programme (819440-TIMP). We also acknowledge financial support from KAMIN program by the Israel Innovation Authority. This work was supported by the Cluster of Excellence Advanced Imaging of Matter (AIM), Grupos Consolidados (IT1249-19) and SFB925. The Flatiron Institute is a division of the Simons Foundation. O.N. gratefully acknowledges the support of the Adams Fellowship Program of the Israel Academy of Sciences and Humanities, support from the Alexander von Humboldt foundation, and support from the Schmidt Science Fellowship.

Disclosures. The authors declare no conflicts of interest.

Data availability. Data underlying the results presented in this paper are not publicly available at this time but may be obtained from the authors upon reasonable request.

Supplemental document. See Supplement 1 for supporting content.

References

1. D. Griffiths, *Introduction to Elementary Particles* (John Wiley & Sons, 2008).
2. D. K. Kondepudi and D. J. Durand, "Chiral asymmetry in spiral galaxies?" Chirality **13**(7), 351–356 (2001).
3. S. Jia, S.-Y. Xu, and M. Z. Hasan, "Weyl semimetals, Fermi arcs and chiral anomalies," Nat. Mater. **15**(11), 1140–1144 (2016).
4. Z. Hanyu, Y. Jun, L. Ming-Yang, X. Jun, Z. Lifa, Y. Chih-Wen, R. A. Kaindl, L. Lain-Jong, W. Yuan, and Z. Xiang, "Observation of chiral phonons," Science **359**(6375), 579–582 (2018).
5. F. Bussolotti, H. Kawai, Z. E. Ooi, V. Chellappan, D. Thian, A. L. C. Pang, and K. E. J. Goh, "Roadmap on finding chiral valleys: screening 2D materials for valleytronics," Nano Futures **2**(3), 032001 (2018).
6. M. Kenji, "Bioactive natural products and chirality," Chirality **23**(6), 449–462 (2011).
7. U. J. Meierhenrich, "Amino Acids and the Asymmetry of Life," Eur. Rev. **21**(2), 190–199 (2013).
8. W. H. Brooks, W. C. Guida, and K. G. Daniel, "The significance of chirality in drug design and development," Curr. Top. Med. Chem. (Sharjah, United Arab Emirates) **11**(7), 760–770 (2011).
9. P. Y. Bruice, *Organic Chemistry*, 5th ed. (Prentice Hall, 2006).
10. "Development of New Stereoisomeric Drugs," https://www.fda.gov/regulatory-information/search-fda-guidance-documents/development-new-stereoisomeric-drugs.
11. N. Berova, P. L. Polavarapu, K. Nakanishi, and R. W. Woody, *Comprehensive Chiroptical Spectroscopy: Applications in Stereochemical Analysis of Synthetic Compounds, Natural Products, and Biomolecules* (John Wiley & Sons, 2012), 2.
12. P. Fischer, D. S. Wiersma, R. Righini, B. Champagne, and A. D. Buckingham, "Three-Wave Mixing in Chiral Liquids," Phys. Rev. Lett. **85**(20), 4253–4256 (2000).
13. G. J. Simpson, "Molecular Origins of the Remarkable Chiral Sensitivity of Second-Order Nonlinear Optics," ChemPhysChem **5**(9), 1301–1310 (2004).
14. M. A. Belkin and Y. R. Shen, "Non-linear optical spectroscopy as a novel probe for molecular chirality," Int. Rev. Phys. Chem. **24**(2), 257–299 (2005).
15. D. Patterson, M. Schnell, and J. M. Doyle, "Enantiomer-specific detection of chiral molecules via microwave spectroscopy," Nature **497**(7450), 475–477 (2013).
16. S. Eibenberger, J. Doyle, and D. Patterson, "Enantiomer-Specific State Transfer of Chiral Molecules," Phys. Rev. Lett. **118**(12), 123002 (2017).
17. C. Pérez, A. L. Steber, S. R. Domingos, A. Krin, D. Schmitz, and M. Schnell, "Coherent Enantiomer-Selective Population Enrichment Using Tailored Microwave Fields," Astron. Astrophys., Suppl. Ser. **56**(41), 12512–12517 (2017).
18. R. Cireasa, A. E. Boguslavskiy, B. Pons, M. C. H. Wong, D. Descamps, S. Petit, H. Ruf, N. Thiré, A. Ferré, J. Suarez, J. Higuet, B. E. Schmidt, A. F. Alharbi, F. Légaré, V. Blanchet, B. Fabre, S. Patchkovskii, O. Smirnova, Y. Mairesse, V. R. Bhardwaj, N. Thire, A. Ferre, J. Suarez, J. Higuet, B. E. Schmidt, A. F. Alharbi, F. Legare, V. Blanchet, B. Fabre, S. Patchkovskii, O. Smirnova, Y. Mairesse, and V. R. Bhardwaj, "Probing molecular chirality on a sub-femtosecond timescale," Nat. Phys. **11**(8), 654–658 (2015).
19. D. Baykusheva and H. J. Wörner, "Chiral Discrimination through Bielliptical High-Harmonic Spectroscopy," Phys. Rev. X **8**(3), 031060 (2018).
20. O. Neufeld, D. Ayuso, P. Decleva, M. Y. Ivanov, O. Smirnova, and O. Cohen, "Ultrasensitive Chiral Spectroscopy by Dynamical Symmetry Breaking in High Harmonic Generation," Phys. Rev. X **9**(3), 031002 (2019).
21. D. Ayuso, O. Neufeld, A. F. Ordonez, P. Decleva, G. Lerner, O. Cohen, M. Ivanov, and O. Smirnova, "Synthetic chiral light for efficient control of chiral light–matter interaction," Nat. Photonics **13**(12), 866–871 (2019).

Optics EXPRESS

22. D. Ayuso, A. F. Ordonez, P. Decleva, M. Ivanov, and O. Smirnova, "Enantio-sensitive unidirectional light bending," Nat. Commun. **12**(1), 3951 (2021).
23. D. Ayuso, A. F. Ordonez, M. Ivanov, and O. Smirnova, "Ultrafast optical rotation in chiral molecules with ultrashort and tightly focused beams," Optica **8**(10), 1243–1246 (2021).
24. O. Neufeld and O. Cohen, "Background-Free Measurement of Ring Currents by Symmetry-Breaking High-Harmonic Spectroscopy," Phys. Rev. Lett. **123**(10), 103202 (2019).
25. S. Giri, A. M. Dudzinski, J. C. Tremblay, and G. Dixit, "Time-dependent electronic current densities in chiral molecules," Phys. Rev. A **102**(6), 063103 (2020).
26. X. Zhu, X. Liu, P. Lan, D. Wang, Q. Zhang, W. Li, and P. Lu, "Anomalous circular dichroism in high harmonic generation of stereoisomers with two chiral centers," Opt. Express **24**(22), 24824–24835 (2016).
27. O. Neufeld, H. Hübener, A. Rubio, and U. De Giovannini, "Strong chiral dichroism and enantiopurification in above-threshold ionization with locally chiral light," Phys. Rev. Res. **3**(3), L032006 (2021).
28. A. Castro, H. Appel, M. Oliveira, C. A. Rozzi, X. Andrade, F. Lorenzen, M. A. L. Marques, E. K. U. Gross, and A. Rubio, "octopus: a tool for the application of time-dependent density functional theory," Phys. Status Solidi **243**(11), 2465–2488 (2006).
29. X. Andrade, D. Strubbe, U. De Giovannini, H. Larsen, M. J. T. Oliveira, J. Alberdi-rodriguez, A. Varas, I. Theophilou, N. Helbig, M. J. Verstraete, L. Stella, F. Nogueira, A. Castro, M. A. L. Marques, and A. Rubio, "Real-space grids and the Octopus code as tools for the development of new simulation approaches for electronic systems," Phys. Chem. Chem. Phys. **17**(47), 31371–31396 (2015).
30. N. Tancogne-Dejean, M. J. T. Oliveira, X. Andrade, H. Appel, C. H. Borca, G. Le Breton, F. Buchholz, A. Castro, S. Corni, A. A. Correa, U. De Giovannini, A. Delgado, F. G. Eich, J. Flick, G. Gil, A. Gomez, N. Helbig, H. Hübener, R. Jestädt, J. Jornet-Somoza, A. H. Larsen, I. V. Lebedeva, M. Lüders, M. A. L. Marques, S. T. Ohlmann, S. Pipolo, M. Rampp, C. A. Rozzi, D. A. Strubbe, S. A. Sato, C. Schäfer, I. Theophilou, A. Welden, and A. Rubio, "Octopus, a computational framework for exploring light-driven phenomena and quantum dynamics in extended and finite systems," J. Chem. Phys. **152**(12), 124119 (2020).
31. J. P. Perdew and A. Zunger, "Self-interaction correction to density-functional approximations for many-electron systems," Phys. Rev. B **23**(10), 5048–5079 (1981).
32. T. T. Luu, Z. Yin, A. Jain, T. Gaumnitz, Y. Pertot, J. Ma, and H. J. Wörner, "Extreme–ultraviolet high–harmonic generation in liquids," Nat. Commun. **9**(1), 3723 (2018).
33. V. Svoboda, Z. Yin, T. T. Luu, and H. J. Wörner, "Polarization measurements of deep- to extreme-ultraviolet high harmonics generated in liquid flat sheets," Opt. Express **29**(19), 30799–30808 (2021).
34. H. Eichmann, A. Egbert, S. Nolte, C. Momma, B. Wellegehausen, W. Becker, S. Long, and J. K. McIver, "Polarization-dependent high-order two-color mixing," Phys. Rev. A **51**(5), R3414–R3417 (1995).
35. S. Long, W. Becker, and J. K. McIver, "Model calculations of polarization-dependent two-color high-harmonic generation," Phys. Rev. A **52**(3), 2262–2278 (1995).
36. D. B. Milošević, W. Becker, and R. Kopold, "Generation of circularly polarized high-order harmonics by two-color coplanar field mixing," Phys. Rev. A **61**(6), 063403 (2000).
37. A. Fleischer, O. Kfir, T. Diskin, P. Sidorenko, and O. Cohen, "Spin angular momentum and tunable polarization in high-harmonic generation," Nat. Photonics **8**(7), 543–549 (2014).
38. O. Kfir, P. Grychtol, E. Turgut, R. Knut, D. Zusin, D. Popmintchev, T. Popmintchev, H. Nembach, J. M. Shaw, A. Fleischer, H. Kapteyn, M. Murnane, and O. Cohen, "Generation of bright phase-matched circularly-polarized extreme ultraviolet high harmonics," Nat. Photonics **9**(2), 99–105 (2015).
39. O. Neufeld, M. Even Tzur, and O. Cohen, "Degree of chirality of electromagnetic fields and maximally chiral light," Phys. Rev. A **101**(5), 053831 (2020).
40. MATLAB, *Version 9.0.0.341360 (R2016a)* (The MathWorks Inc., 2016).
41. A. Paszke, S. Gross, F. Massa, A. Lerer, J. Bradbury, G. Chanan, T. Killeen, Z. Lin, N. Gimelshein, and L. Antiga, "Pytorch: An imperative style, high-performance deep learning library," Adv. Neural Inf. Process. Syst. **32**, 8026–8037 (2019).
42. Y. Lecun, L. Bottou, Y. Bengio, and P. Haffner, "Gradient-based learning applied to document recognition," Proc. IEEE **86**(11), 2278–2324 (1998).
43. D. P. Kingma and J. Ba, "Adam: A method for stochastic optimization," arXiv Prepr. arXiv1412.6980 (2014).
44. O. E. Alon, V. Averbukh, and N. Moiseyev, "Selection Rules for the High Harmonic Generation Spectra," Phys. Rev. Lett. **80**(17), 3743–3746 (1998).
45. O. Neufeld, D. Podolsky, and O. Cohen, "Floquet group theory and its application to selection rules in harmonic generation," Nat. Commun. **10**(1), 405 (2019).
46. A. A. Zyuzin and A. A. Burkov, "Topological response in Weyl semimetals and the chiral anomaly," Phys. Rev. B **86**(11), 115133 (2012).
47. M. Z. Hasan, G. Chang, I. Belopolski, G. Bian, S.-Y. Xu, and J.-X. Yin, "Weyl, Dirac and high-fold chiral fermions in topological quantum matter," Nat. Rev. Mater. **6**(9), 784–803 (2021).
48. H. Hübener, M. A. Sentef, U. De Giovannini, A. F. Kemper, and A. Rubio, "Creating stable Floquet–Weyl semimetals by laser-driving of 3D Dirac materials," Nat. Commun. **8**(1), 13940 (2017).
49. D. Baykusheva, D. Zindel, V. Svoboda, E. Bommeli, M. Ochsner, A. Tehlar, and H. J. Wörner, "Real-time probing of chirality during a chemical reaction," Proc. Natl. Acad. Sci. **116**(48), 23923–23929 (2019).